Change Detection Based on Gabor Wavelet Features for Very High Resolution Remote Sensing Images

Zhenxuan Li, Wenzhong Shi, Hua Zhang, and Ming Hao

***Abstract*— In this letter, we propose a change detection method based on Gabor wavelet features for very high resolution (VHR) remote sensing images. First, Gabor wavelet features are extracted from two temporal VHR images to obtain spatial and contextual information. Then, the Gabor-wavelet-based difference measure (GWDM) is designed to generate the difference image. In GWDM, a new local similarity measure is defined, in which the Markov random field neighborhood system is incorporated to obtain a local relationship, and the coefficient of variation method is applied to discriminate contributions from different features. Finally, the fuzzy c-means cluster algorithm is employed to obtain the final change map. Experiments employing QuickBird and SPOT5 images demonstrate the effectiveness of the proposed approach.**

***Index Terms*— Change detection, coefficient of variation, fuzzy c-means (FCM), Gabor wavelet, Markov random field (MRF), remote sensing, very high resolution (VHR).**

I. Introduction

REMOTE sensing change detection identifies changes occurring on the earth's surface by jointly processing multitemporal images acquired from the same geographical area at different times [1]–[3]. This technique has become an increasingly popular research topic due to its relevant and practical applications, including deforestation, damage assessment, disaster monitoring, and urban expansion [4]. In the past decades, a variety of change detection approaches have been developed. Generally, these approaches can be divided into two steps: difference generation and analysis. The difference generation methods include image differencing, image ratio and change vector analysis (CVA) [5], while the analysis step adopts threshold-based methods [6], [7] and clustering-based methods [8], [9]. With the emergence of very high resolution (VHR) remote sensing images, more detailed ground information can be obtained. However, increasing spatial resolution always leads to a reduction in the ability to distinguish spectral statistics between different classes. The conventional change detection methods only utilize spectral information regardless of spatial information, which is inadequate for VHR remote sensing image change detection. Nonetheless, VHR remote sensing images contain abundant spatial and contextual information, which can aid in accurate change detection.

In order to take full advantage of the spatial information in remote sensing images, many feature based methods have been developed, such as line feature [10], shape feature [11], gray level co-occurrence matrix (GLCM) textures [12], and Gabor wavelet features [13]–[15]. Among them, Gabor wavelet features have strong discriminating power and can achieve comparable performance at very low computation cost for change detection [13]. Gong *et al*. [13] performed a robust principal component analysis technique to separate irrelevant and noisy elements from Gabor responses for change detection. In [14], a Gabor filter was utilized to extract spatial and contextual features at different scales and orientations, and a novel post-classification change detection method was proposed using this information. In [15], a simple yet effective unsupervised change detection approach was designed for multitemporal synthetic aperture radar images by jointly exploiting the robust Gabor wavelet representation and advanced cascade clustering.

Although effort has been made to improve Gabor feature based methods, practical and effective method needs to be developed. In [15], the Gabor features were extracted from the difference image, which can be obtained using CVA applied to two temporal images. However, a significant quantity of spatial and contextual information contained in VHR images cannot be extracted this way, due to loss of information in the differencing process. In addition, the pixelwise difference measure (i.e., CVA) is not suitable for Gabor wavelet features due to lack of spatial correlation. Therefore, an effective difference measure based on Gabor features is proposed based on extracted Gabor features from original images.

In this letter, a change detection method based on Gabor wavelet features is proposed for VHR images. The main contributions consist of two parts. First, a new Gabor-based change detection procedure is designed based on the Gabor wavelet features, which were extracted from the two original temporally different VHR images. Second, a Gabor-wavelet-based difference measure (GWDM) is proposed, in which the spatial correlation of the Gabor features is fully considered using a Markov random field (MRF) [16] neighborhood system. Weights between different features are also taken into account using coefficient of variation method (CVM) [17] according to their contributions.

This letter is organized as follows. Section II describes the proposed change detection approach. Section III presents

Manuscript received September 22, 2016; revised February 15, 2017; accepted March 7, 2017. This work was supported in part by the National Natural Science Foundation of China under Grant 41331175, in part by the Priority Academic Program Development of Jiangsu Higher Education Institutions, in part by the Fundamental Research Funds for the Central Universities under Grant 2015XKQY09, and in part by the Natural Science Foundation of Jiangsu Province under Grant BK20160248. *(Corresponding author: Wenzhong Shi.)*

Z. Li, H. Zhang, and M. Hao are with the School of Environment Science and Spatial Informatics, China University of Mining and Technology, Xuzhou 221116, China (e-mail: zxlicumt@126.com; zhhuamesi@gmail.com; haomingcumt@gail.com).

W. Shi is with the Department of Land Surveying and Geo-Informatics, The Hong Kong Polytechnic University, Hong Kong (e-mail: lswzshi@polyu.edu.hk).

Color versions of one or more of the figures in this letter are available online at http://ieeexplore.ieee.org.

Digital Object Identifier 10.1109/LGRS.2017.2681198

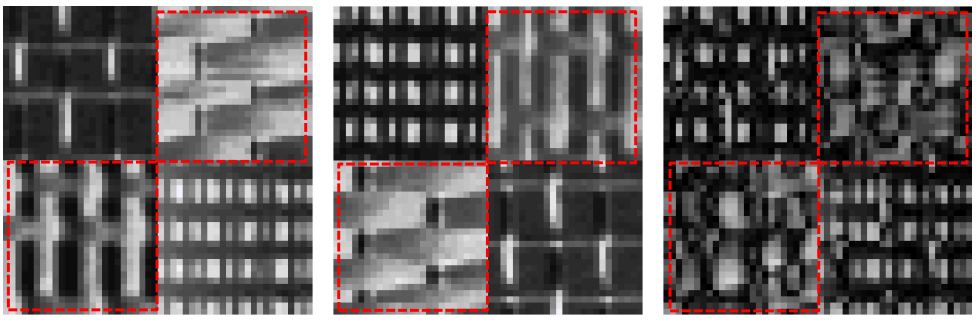

(a) (b) (c)

Fig. 1. (a) Simulated image chip at time t_1. (b) Simulated image chip at time t_2. (c) Difference image generated by subtracting the two image chips.

the experiments and analysis, and Section IV provides the conclusions.

II. Change Detection Based on Gabor Wavelet Features for VHR Images

A. Problem Formulation

Supposing two co-registered and radiometrically corrected VHR remote sensing images acquired over the same geographical area at times t_1 and t_2. Let X_1 and X_2 be the two images, which have the same size, $M \times N$. As shown in Fig. 1(a) and (b), two corresponding simulated image chips were acquired from the original images X_1 and X_2, respectively. The difference image generated by subtracting the two images chips is shown in Fig. 1(c).

To demonstrate the necessity of Gabor feature extraction prior to the differencing process, a theoretical analysis is provided as follows. As seen in Fig. 1, the two temporally different original image chips have abundant spatial and contextual information, but the difference image has little, i.e., the area inside the dotted line in Fig. 1. A significant amount of structural information was lost in the differencing process. As a result, many features included in the original images cannot be extracted and applied for change detection.

After Gabor feature extraction from the original images, a difference measure is needed to detect the changes based on multiple features in the two images. The pixelwise difference measure (i.e., CVA) is not suitable for images including the strong spatial correlation inside the features. As shown in Fig. 2(a) and (b), two corresponding Gabor feature image chips were obtained and the difference image generated by CVA is shown in Fig. 2(c). Focusing on the image regions highlighted by white boxes in Fig. 2 reveals the problem with this method. According to traditional methods, this region will be directly classified into an unchanged class. However, this result is not completely correct because the two temporal feature image chips were not coincident.

To address the aforementioned problems, a novel change detection method based on Gabor wavelet features is proposed for VHR remote sensing images in this letter. As shown in Fig. 3, the proposed approach consists of three blocks as follows. First, Gabor wavelet features were extracted from two temporal VHR remote sensing images, respectively. Then, a GWDM was designed to generate the difference image. Finally, the fuzzy c-means (FCM) cluster algorithm [9] was implemented to generate the final change map. Detailed descriptions are provided in Sections II-B–II-D.

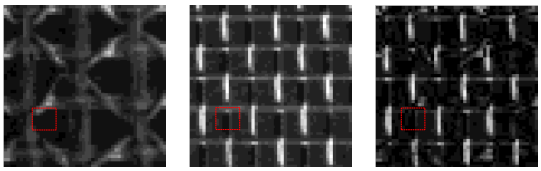

(a) (b) (c)

Fig. 2. (a) Gabor feature of simulated image chip at time t_1. (b) Gabor feature of simulated image chip at time t_2. (c) Difference image generated by CVA.

B. Gabor Wavelet Features Extraction

The Gabor wavelet can be considered a wavelet transform, in which the Gabor function is utilized as the mother wavelet. The 2-D Gabor function $g(x, y)$ is written as

$$g(x, y) = \left(\frac{1}{2\pi\sigma_x\sigma_y}\right)\exp\left[-\frac{1}{2}\left(\frac{x^2}{\sigma_x^2}+\frac{y^2}{\sigma_y^2}\right)+2\pi j W x\right] \tag{1}$$

where σ_x and σ_y denote the standard deviation of the primary Gabor function of Gabor along the x and y axis, respectively, and $j = \sqrt{-1}$ and W denote the frequency bandwidth of the Gabor wavelet. Its Fourier transform $G(u, v)$ is expressed as

$$G(u, v) = \exp\left\{-\frac{1}{2}\left[\frac{(u-W)^2}{\sigma_u^2}+\frac{v^2}{\sigma_v^2}\right]\right\} \tag{2}$$

where $\sigma_u = 1/2\pi\sigma_x$ and $\sigma_v = 1/2\pi\sigma_y$. Let $g(x, y)$ be the mother Gabor wavelet, then a set of self-similar Gabor filter can be generated by proper scale and rotation transformation for $g(x, y)$. The filters can be denoted as

$$g_{mn}(x, y) = a^{-m}G(x', y'), \quad a > 1, m, n = \text{integer} \tag{3}$$

where $x' = a^{-m}(x\cos\theta + y\sin\theta)$, $y' = a^{-m}(-x\sin\theta + y\cos\theta)$, $\theta = n\pi/K$, and K is the total number of orientations, $n \in [0, K-1]$. a^{-m} is the scale factor, $m \in [0, S-1]$, and S is the total number of scales.

In order to decrease the redundant information among the Gabor features, the parameters of the Gabor wavelet are set as follows:

$$a = (U_h/U_l)^{-\frac{1}{S-1}}, \quad \sigma_u = \frac{(a-1)U_h}{(a+1)\sqrt{2\ln 2}}$$
$$\sigma_v = \tan\left(\frac{\pi}{2k}\right)\left[U_h - 2\ln\left(\frac{\sigma_u^2}{U_h}\right)\right]\left[2\ln 2 - \frac{(2\ln 2)^2\sigma_u^2}{U_h^2}\right]^{-\frac{1}{2}} \tag{4}$$

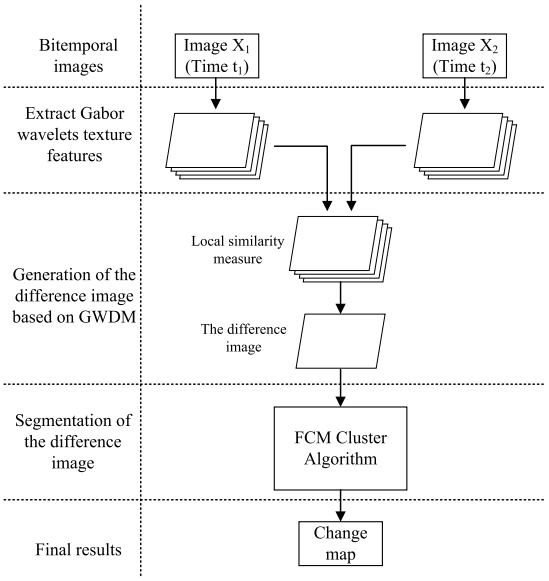

Fig. 3. Framework of the proposed change detection approach.

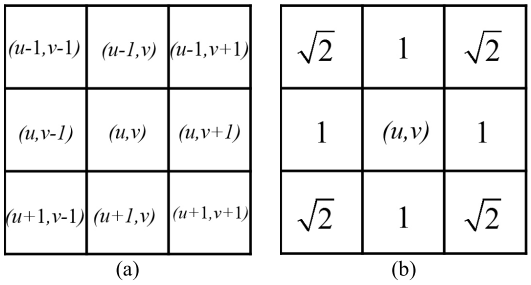

Fig. 4. (a) Neighborhood system centered at (*u, v*). (b) Distance between the center pixel (*u, v*) and its neighborhoods.

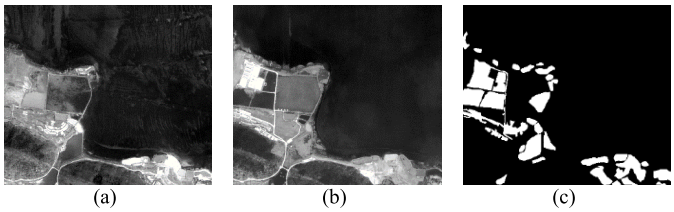

Fig. 5. QuickBird data set. (a) QuickBird image from 2002. (b) QuickBird image from 2009. (c) Ground truth image.

where U_l and U_h denote the lower and upper center frequencies of interest.

Given an image *I(x, y)*, its 2-D Gabor wavelet transform can be defined as

$$W_{mn}(x, y) = \int I(x_1, y_1) g_{mn}{}^*(x - x_1, y - y_1) dx_1 dy_1 \quad (5)$$

where * denotes the complex conjugate. As such, the Gabor wavelet features $W_{mn}(x,y)$ are extracted from the VHR remote sensing images.

C. Gabor-Wavelet-Based Difference Measure

After Gabor feature extraction, the GWDM is defined to generate the difference image. In GWDM, based on the MRF neighborhood system between two temporal Gabor features, a local similarity measure $S_{mn}(t_1, t_2)$ is designed and formulated as

$$S_{mn}(t_1, t_2) = \frac{1}{1 + d_{mn}(t_1, t_2)} \quad (6)$$

in which we have (7), as shown at the bottom of the page, where $d_{mn}(t_1, t_2)$ denotes the variation index between two temporally corresponding Gabor feature regions at scale m and orientation n. $W_{mn}^{t_1}(u, v)$ and $W_{mn}^{t_2}(u, v)$ present Gabor wavelet features at times t_1 and t_2, respectively. *(u,v)* denotes the position of the target pixel in the image. ω defines the MRF neighborhood system as centered at the target pixel, as shown in Fig. 4(a). h denotes the distance between the target pixel and its neighboring pixels, as shown in Fig. 4(b).

Using the local similarity measure, the similarity images at each scale and orientation are generated from the two temporal Gabor wavelet features. In order to display the contributions of different Gabor features, a weight determination method, namely, CVM, is utilized in this letter. In CVM, the weights of each feature can be calculated as

$$w_{mn} = \frac{V_{mn}}{\sum_m^S \sum_n^K V_{mn}}, \quad \text{and } V_{mn} = \frac{\sigma_{mn}}{\mu_{mn}} \quad (8)$$

where V_{mn} presents the coefficient of variation of the Gabor feature at scale m and orientation n, and μ_{mn} and σ_{mn} are the mean value and the standard deviation of this feature, respectively. Then, the difference image can be generated as

$$D(t_1, t_2) = \sum_m^S \sum_n^K \frac{w_{mn}}{S_{mn}(t_1, t_2)}. \quad (9)$$

In this way, the difference image is obtained using GWDM.

D. Segmentation of the Difference Image

Once the difference image has been generated, change detection processing is needed to classify the changed pixels and unchanged pixels by segmenting the difference image. In this letter, the FCM cluster algorithm [9] is utilized to generate the final change map. FCM is one of the most important fuzzy clustering algorithms [18], [19], and many studies have improved it for difference images analysis [8], [20]. The FCM cluster algorithm attempts to find fuzzy partitioning of a given image by minimizing the objective functional

$$J(U, c_1, c_2, \ldots, c_c) = \sum_{i=1}^{c} \sum_{j}^{n} u_{ij}^m d_{ij}^2 \quad (10)$$

where $U = [u_{ij}]$ is the membership probability matrix of X, and c_i denotes the center of the ith cluster. $d_{ij} = \| c_i -$

$$d_{mn}(t_1, t_2) = \sqrt{\left(\left[W_{mn}^{t_1}(u, v) - W_{mn}^{t_2}(u, v) \right]^2 + \sum_{(u,v) \in \omega} \left(\frac{W_{mn}^{t_1}(u, v) - W_{mn}^{t_2}(u, v)}{h} \right)^2 \right)} \quad (7)$$

(a) (b) (c)

Fig. 6. SPOT5 data set. (a) SPOT5 image from 2008. (b) SPOT5 image from 2009. (c) Ground truth image.

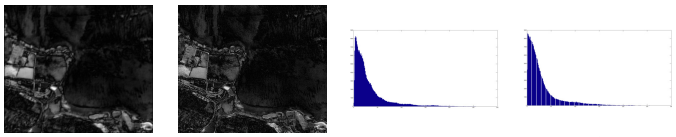

(a) (b) (c) (d)

Fig. 7. Difference images and corresponding histograms of QuickBird data set. (a) Difference image based on GWDM with the QuickBird image. (b) Difference image based on CVA with the QuickBird image. (c) Histogram of the difference image based on GWDM. (d) Histogram of the difference image based on CVA.

$x_j \parallel$ denotes the Euclidean distance between the ith cluster and jth pixel. $m \in [1, \infty]$ denotes the weighting exponent. By minimizing this function, the membership probability can be obtained and final change map is generated.

III. Experiments and Analysis

In order to evaluate the performance of the proposed approach, two temporal VHR remote sensing images were used. Three indices in terms of experimental result and ground truth were adopted for quantitative evaluation, such as the false alarm rate P_F, missed detection rate P_M and total error rate P_T. Specifically, $P_F = N_f/N_u$, where N_f is the number of changed pixels in the change detection result that were classified as the unchanged class in the ground truth image, and N_u is the total number of unchanged pixels counted in the ground truth image. $P_M = N_m/N_c$, where N_m is the number of unchanged pixels in the change detection result that were classified as the changed class in the ground truth image, and N_c is the total number of changed pixels counted in the ground truth image. $P_T = (N_m + N_f)/(N_c + N_u)$.

To demonstrate the performance of the proposed method, comparisons between the proposed algorithm and traditional change detection algorithms were implemented. Because CVA is the most popular difference image generation method and can provide more detailed change information [2], it was selected to compare with the proposed GWDM in this letter. For the difference image segmentation method, the expectation maximization (EM) based algorithm was adopted to compare with the FCM cluster algorithm.

A. Description of the Data Sets and Experimental Setup

The first data set contains two VHR images of size 470 × 548 pixels acquired by the QuickBird satellite covering the city of Wuhan, China, on April 1, 2002 and July 16, 2009, as shown in Fig. 5(a) and (b). The image spatial resolution is 2.4 m. The main land cover types are water, grass, road, and building. The ground truth image of the data set is shown in Fig. 5(c), which was generated by visual interpretation. The second data set (600 × 600) was obtained

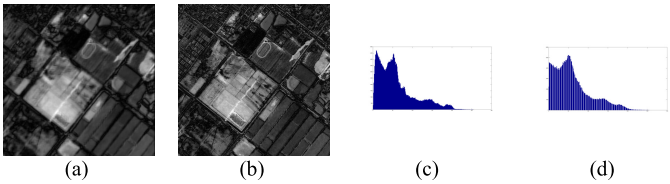

(a) (b) (c) (d)

Fig. 8. Difference images and corresponding histograms of SPOT5 data set. (a) Difference image based on GWDM with the SPOT5 image. (b) Difference image based on CVA with the SPOT5 image. (c) Histogram of the difference image based on GWDM. (d) Histogram of the difference image based on CVA.

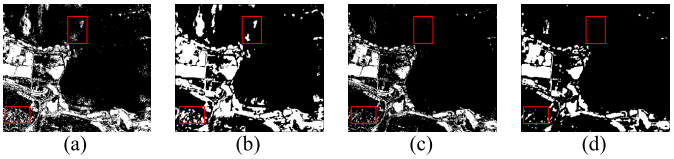

(a) (b) (c) (d)

Fig. 9. Change detection results for the different methods with the QuickBird imagery. (a) CVA–EM. (b) CVA–FCM. (c) GWDM–EM. (d) GWDM–FCM.

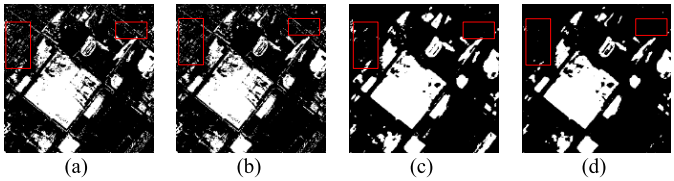

(a) (b) (c) (d)

Fig. 10. Change detection results for the different methods with the SPOT5 imagery. (a) CVA–EM. (b) CVA–FCM. (c) GWDM–EM. (d) GWDM–FCM.

by Satellite Probatoire d'Observation de la Terre 5 (SPOT5) covering the city of Tianjin, China, on April 24, 2008 and February 23, 2009; the images were generated by fusing panchromatic and multispectral images. The spatial resolution of this data set is 2.5 m. the main land cover types are farmland, road and building. The ground truth for the change detection map shown in Fig. 6(c) was manually created based on visual interpretation of the images shown in Fig. 6(a) and (b).

In the two experiments, the relevant parameters were set as follows. In Gabor wavelet feature extraction, some parameters were implemented using default parameters, such as $U_l = 0.05$, $U_h = 0.4$, $S = 4$, and $K = 6$. The window size of the Gabor filter was chosen based on experiences. The window sizes in the QuickBird and SPOT5 experiments were 5 and 9, respectively. In the FCM cluster algorithm, the initial membership probability was randomly generated with uniformly distributed values in (0, 1), $c = 2$, $m = 2$, $\varepsilon = 1e - 5$, and the maximum number of iterations was 200.

B. Experimental Results and Analysis

Figs. 7 and 8 show the difference image and corresponding histograms generated from the QuickBird and SPOT5 data sets, respectively. Specifically, Figs. 7(c) and 8(c) present histograms of the difference images produced using GWDM, and Figs. 7(d) and 8(d) show the histograms of the difference images produced using CVA. As shown in Figs. 7 and 8, the GWDM histogram distributions are more balanced than those using CVA. This observation indicates that more details in the difference image are preserved utilizing GWDM.

Figs. 9(a)–(d) and 10(a)–(d) show the change detection results using CVA–EM, CVA–FCM, GWDM–EM and the proposed GWDM–FCM method for the QuickBird and SPOT5 images, respectively. Visual comparisons of the four change

TABLE I
COMPARISIONS OF THE DIFFERENT CHANGE DETECTION APPROACHES WITH THE QUICKBIRD IMAGE

Method	False Alarms		Missed Detections		Total Errors	
	pixels	P_F (%)	pixels	P_M (%)	pixels	P_T (%)
CVA-EM	28598	12.63	4925	15.78	33523	13.02
CVA-FCM	32127	14.19	3465	11.11	35592	13.82
GWDM-EM	11295	4.99	8011	25.68	19306	7.5
GWDM-FCM	10780	4.76	6762	21.67	17542	6.81

TABLE II
COMPARISIONS OF THE DIFFERENT CHANGE DETECTION APPROACHES WITH THE SPOT5 IMAGE

Method	False Alarms		Miss Detections		Total Errors	
	pixels	P_F (%)	pixels	P_M (%)	pixels	P_T (%)
CVA-EM	19400	7.24	19388	21.09	38788	10.77
CVA-FCM	17953	6.7	20155	21.92	38108	10.59
GWDM-EM	14666	5.47	13273	14.44	27939	7.76
GWDM-FCM	5520	2.06	17993	19.57	23513	6.53

detection approaches generally indicate the performance of each change detection method. Compared with the ground truth images in Figs. 5(c) and 6(c), GWDM–EM and our proposed method GWDM–FCM have better visual change detection results and have fewer error pixels. Compared with traditional change detection methods shown in Figs. 9(a) and (b) and 10(a) and (b), the Gabor-based approaches show significant improvements. These are highlighted by white boxes in Figs. 9(c) and (d) and 10(c) and (d). The results indicate that the spatial contextual information generated by the Gabor wavelet features can effectively decrease the false alarm rate and improve the final change detection results.

Tables I and II show the P_F, P_M, and P_T values of the four change detection approaches from the QuickBird and SPOT5 data sets. As shown in Tables I and II, the GWDM–EM and our proposed GWDM–FCM method outperform the CVA–EM and CVA–FCM methods in change detection performance. Specifically, for the QuickBird data set, the total error rates for GWDM–EM and GWDM–FCM improved 5.52% and 7.01% over CVA–EM and CVA–FCM, respectively. For the SPOT5 data set, the total error rates for GWDM–EM and GWDM–FCM were, respectively, improved by 3.01% and 4.06% over CVA-EM and CVA–FCM. In addition, the proposed GWDM–FCM method provides better performance than GWDM–EM base on the two data sets. This indicates that the proposed cascade scheme is helpful for discriminating changed and unchanged pixels, and is more accurate than traditional methods. In addition, the quantitative comparison results are corroborated by the visual comparison results.

IV. CONCLUSION

A novel change detection technique based on Gabor wavelet features is proposed and implemented for VHR remote sensing images in this letter. The proposed algorithm extracts Gabor wavelet features from two temporal VHR images before the differencing process to obtain spatial and contextual information. A GWDM based on MRF and CVM is then proposed and used to generate the difference image. Finally, the FCM cluster algorithm is applied to obtain the final change map. The effectiveness of the proposed approach is evaluated using QuickBird and SPOT5 images and the results show that the proposed method has the ability to provide better change detection results for VHR images than traditional methods. Future work will be devoted to feature selection and automatic determination of parameters.

REFERENCES

[1] L. Bruzzone and F. Bovolo, "A novel framework for the design of change-detection systems for very-high-resolution remote sensing images," *Proc. IEEE*, vol. 101, no. 3, pp. 609–630, Mar. 2013.
[2] D. Lu, P. Mausel, E. Brondízio, and E. Moran, "Change detection techniques," *Int. J. Remote Sens.*, vol. 25, no. 12, pp. 2365–2401, Jun. 2004.
[3] A. P. Tewkesbury, A. J. Comber, N. J. Tate, A. Lamb, and P. F. Fisher, "A critical synthesis of remotely sensed optical image change detection techniques," *Remote Sens. Environ.*, vol. 160, pp. 1–14, Apr. 2015.
[4] M. Hussain, D. Chen, A. Cheng, H. Wei, and D. Stanley, "Change detection from remotely sensed images: From pixel-based to object-based approaches," *ISPRS J. Photogramm. Remote Sens.*, vol. 80, pp. 91–106, Jun. 2013.
[5] R. D. Johnson and E. S. Kasischke, "Change vector analysis: A technique for the multispectral monitoring of land cover and condition," *Int. J. Remote Sens.*, vol. 19, no. 3, pp. 411–426, Mar. 1998.
[6] L. Bruzzone and D. F. Prieto, "Automatic analysis of the difference image for unsupervised change detection," *IEEE Trans. Geosci. Remote Sens.*, vol. 38, no. 3, pp. 1171–1182, May 2000.
[7] P. He, W. Shi, H. Zhang, and M. Hao, "A novel dynamic threshold method for unsupervised change detection from remotely sensed images," *Remote Sens. Lett.*, vol. 5, no. 4, pp. 396–403, Apr. 2014.
[8] M. Hao, H. Zhang, W. Shi, and K. Deng, "Unsupervised change detection using fuzzy *c*-means and MRF from remotely sensed images," *Remote Sens. Lett.*, vol. 4, no. 12, pp. 1185–1194, Dec. 2013.
[9] A. Ghosh, N. S. Mishra, and S. Ghosh, "Fuzzy clustering algorithms for unsupervised change detection in remote sensing images," *Inf. Sci.*, vol. 181, no. 4, pp. 699–715, Feb. 2011.
[10] N. C. Rowe and L. L. Grewe, "Change detection for linear features in aerial photographs using edge-finding," *IEEE Trans. Geosci. Remote Sens.*, vol. 39, no. 7, pp. 1608–1612, Jul. 2001.
[11] J. Li and R. M. Narayanan, "A shape-based approach to change detection of lakes using time series remote sensing images," *IEEE Trans. Geosci. Remote Sens.*, vol. 41, no. 11, pp. 2466–2477, Nov. 2003.
[12] P. C. Smits and A. Annoni, "Toward specification-driven change detection," *IEEE Trans. Geosci. Remote Sens.*, vol. 38, no. 3, pp. 1484–1488, May 2000.
[13] M. Gong, Y. Li, L. Jiao, M. Jia, and L. Su, "SAR change detection based on intensity and texture changes," *ISPRS J. Photogramm. Remote Sens.*, vol. 93, pp. 123–135, Jul. 2014.
[14] G. Camps-Valls, L. Gomez-Chova, J. Muñoz-Mari, L. Alonso, J. Calpe-Maravilla, and J. Moreno, "Multitemporal image classification and change detection with kernels," *Proc. SPIE*, vol. 6365, p. 63650H, Sep. 2006.
[15] H.-C. Li, T. Celik, N. Longbotham, and W. J. Emery, "Gabor feature based unsupervised change detection of multitemporal SAR images based on two-level clustering," *IEEE Geosci. Remote Sens. Lett.*, vol. 12, no. 12, pp. 2458–2462, Dec. 2015.
[16] S. Krishnamachari and R. Chellappa, "Multiresolution Gauss–Markov random field models for texture segmentation," *IEEE Trans. Image Process.*, vol. 6, no. 2, pp. 251–267, Feb. 1997.
[17] S.-T. Liu, "A mathematical programming approach to sample coefficient of variation with interval-valued observations," *TOP*, vol. 24, no. 1, pp. 1–18, Apr. 2015.
[18] D. E. Gustafson and W. C. Kessel, "Fuzzy clustering with a fuzzy covariance matrix," in *Proc. IEEE CDC*, vol. 2. Jan. 1979, pp. 761–766.
[19] J. C. Bezdek, *Pattern Recognition With Fuzzy Objective Function Algorithms*. New York, NY, USA: Plenum, 1981.
[20] W. Ma, L. Jiao, M. Gong, and C. Li, "Image change detection based on an improved rough fuzzy c-means clustering algorithm," *Int. J. Mach. Learn. Cybern.*, vol. 5, no. 3, pp. 369–377, Jun. 2014.